Solution of the Bethe-Salpeter equation without empty electronic states: Application to the absorption spectra of bulk systems

Dario Rocca, Yuan Ping, Ralph Gebauer, and Giulia Galli

Phys. Rev. B **85**, 045116 — Published 17 January 2012

DOI: 10.1103/PhysRevB.85.045116

Solution of the Bethe-Salpeter equation without empty electronic states: application to the absorption spectra of bulk systems

Dario Rocca,[1,*] Yuan Ping,[1] Ralph Gebauer,[2,3] and Giulia Galli[1,4]

[1]*Department of Chemistry, University of California, Davis, California, 95616*
[2] *The Abdus Salam International Centre for Theoretical Physics (ICTP), Strada Costiera 11, 34151 Trieste, Italy*
[3] *CNR-IOM DEMOCRITOS Simulation Center, 34136 Trieste, Italy*
[4]*Department of Physics, University of California, Davis, California 95616*

(Dated: January 3, 2012)

An approach recently developed to solve the Bethe-Salpeter equation within density matrix perturbation theory is extended to the calculation of optical spectra of periodic systems. This generalization requires numerical integrations within the first Brillouin Zone, that are efficiently performed by exploiting point group symmetries. The technique is applied to the calculation of the optical spectra of bulk Si, diamond C and cubic SiC. Numerical convergence and the accuracy of the Tamm-Dancoff approximation are discussed in detail.

PACS numbers:

I. INTRODUCTION

The ability to compute optical absorption spectra from first principles is of fundamental importance both to complement and help interpret experiments and to predict the properties of new materials[1,2]. For example calculations of absorption spectra may be instrumental in the search of photoelectrodes with optimal sunlight absorption for solar cell applications[3,4]. It is thus desirable to develop theoretical methods and computational techniques to obtain absorption spectra that are both accurate and scalable to systems with a large number of atoms.

Two widely used approaches to compute *ab initio* optical absorption spectra are time-dependent functional theory (TDDFT)[5] and many-body perturbation theory (MBPT)[1]. When local or semi-local exchange-correlation functionals are used, time-dependent density functional theory may be applied to relatively large systems (up to thousands of electrons) and it has been proven to be accurate for several molecules. However, the most commonly used local approximations for the TDDFT kernel poorly describe the optical properties of extended periodic solids and nanostructures[1]. Within MBPT, the GW approximation (where G indicates the single-particle Green's function and W the screened Coulomb potential) has been used to compute quasi-particle energies and the Bethe-Salpeter equation (BSE) solved to compute optical spectra. The GW/BSE approach is computationally more expensive than TDDFT but it overcomes some of the limitations of local TDDFT, e.g., in the description of excitons in periodic systems[1,6–8] and of charge transfer excitations in molecules[9]. Standard techniques to solve the BSE make use of an electron-hole basis set[7], that requires the explicit calculation of a large number of unoccupied electronic states, and the evaluation of a large number of exchange integrals between valence and conduction states.

Recently we have proposed a method to solve the BSE that does not require the explicit calculation of empty states[9]. This approach combines ideas proposed in the context of TDDFT[10,11] and techniques to represent the dielectric matrix[12,13] based on density functional perturbation theory[14]. The evaluation of the BSE kernel involves a number of orbitals equal to the number of occupied states (N_v) and numerically it scales as ground-state Hartree-Fock calculations (see Sec. II). The approach developed in Ref. [9] makes efficient use of iterative solvers and matrix by vector multiplications are performed by using fast Fourier transform techniques, without building and storing explicitly neither the BSE Hamiltonian nor dielectric matrices.

In this work we generalize the formalism of Ref.[9] to periodic systems, and thus we include proper integrations over the first Brillouin zone. The method is then applied to the study of the optical properties of bulk silicon, carbon diamond and cubic silicon carbide. The convergence with respect to several numerical parameters and the comparison with previous results[6–8] are extensively discussed.

The rest of the paper is organized as follow. In Sec. II the BSE formalism for periodic systems is presented within a density matrix framework and the techniques used to avoid the explicit inclusion of empty states are illustrated. In Sec. III we show how the symmetry of the system can be used to accelerate the solution of the BSE. In Sec. IV we present the application of the method to the calculation of the optical absorption spectra of bulk silicon, carbon diamond and cubic silicon carbide, and we compare our results with previous calculations. Sec. V contains our conclusions, and in Appendix A we give some details of the implementation of time-reversal symmetry operations.

II. THEORY

The density matrix perturbation theory formulation of the BSE has been introduced in Ref.[9]. Here we present in detail its extension to periodic systems. Because of several formal analogies, the derivation given below can be easily extended to the

TDDFT formulation presented in Refs.[10,11,15], including not only (semi-)local exchange-correlation functionals but also hybrid functionals.

The starting point of our derivation is the quantum-Liouville equation for density matrices written in the Coulomb-hole plus screened-exchange (COHSEX) approximation[16]:

$$i\frac{d\hat{\rho}_{\mathbf{k}}(t)}{dt} = \left[\hat{H}_{COHSEX}(t), \hat{\rho}_{\mathbf{k}}(t)\right], \tag{1}$$

where the square brackets indicate commutators and a hat denotes quantum-mechanical operators; within a real space representation, $\rho_{\mathbf{k}}(\mathbf{r},\mathbf{r}',t) = \sum_v \phi_{v\mathbf{k}}(\mathbf{r},t)\phi^*_{v\mathbf{k}}(\mathbf{r}',t)$ and the density matrix is given by:

$$\rho(\mathbf{r},\mathbf{r}',t) = \sum_{\mathbf{k}\in BZ} w_{\mathbf{k}}\rho_{\mathbf{k}}(\mathbf{r},\mathbf{r}',t) = \sum_v \sum_{\mathbf{k}\in BZ} w_{\mathbf{k}}\phi_{v\mathbf{k}}(\mathbf{r},t)\phi^*_{v\mathbf{k}}(\mathbf{r}',t), \tag{2}$$

$\mathbf{k}$ denotes a point in the Brillouin zone (BZ) and $\phi_{v\mathbf{k}}(\mathbf{r},t)$ are single particle occupied Bloch orbitals. In the following we will adopt the notation $\rho(\mathbf{r},t)$ to indicate $\rho(\mathbf{r},\mathbf{r},t)$. In Eq. 2 we have substituted the integral over the BZ with a summation over a discrete set of k-points:

$$\frac{1}{\Omega_{BZ}}\int_{\Omega_{BZ}} d\mathbf{k} \longrightarrow \sum_{\mathbf{k}\in BZ} w_{\mathbf{k}} \tag{3}$$

where $w_{\mathbf{k}}$ weighs the contribution of each k-point $\mathbf{k}$ and Ω_{BZ} is the BZ volume.

The time-dependent quasi-particle Hamiltonian operator applied to a valence state, in Hartree atomic units and within the COHSEX approximation is:

$$\begin{aligned}\int \hat{H}_{COHSEX}(\mathbf{r},\mathbf{r}',t)\phi_{v\mathbf{k}}(\mathbf{r}',t)\,d\mathbf{r}' = &\left(-\frac{1}{2}\nabla^2 + v_H(\mathbf{r},t) + v_{ext}(\mathbf{r},t)\right)\phi_{v\mathbf{k}}(\mathbf{r},t) \\ &+ \int \Sigma_{COHSEX}(\mathbf{r},\mathbf{r}',t)\phi_{v\mathbf{k}}(\mathbf{r}',t)d\mathbf{r}',\end{aligned} \tag{4}$$

where v_{ext} is an external time-dependent periodic potential,

$$v_H(\mathbf{r}) = \int \rho(\mathbf{r}',t)v(\mathbf{r},\mathbf{r}')d\mathbf{r}' \tag{5}$$

is the Hartree potential, and $\Sigma_{COHSEX} = \Sigma_{COH} + \Sigma_{SEX}$ is the self-energy in the COHSEX approximation

$$\int \Sigma_{COH}(\mathbf{r},\mathbf{r}')\phi_{v\mathbf{k}}(\mathbf{r}',t)d\mathbf{r}' = \frac{1}{2}\int \delta(\mathbf{r}-\mathbf{r}')W_p(\mathbf{r}',\mathbf{r};\mathbf{k})\phi_{v\mathbf{k}}(\mathbf{r}',t)d\mathbf{r}' \tag{6}$$

$$\int \Sigma_{SEX}(\mathbf{r},\mathbf{r}',t)\phi_{v\mathbf{k}}(\mathbf{r}',t)d\mathbf{r}' = -\sum_{v'}\sum_{\mathbf{k}'\in BZ}\int \phi_{v'\mathbf{k}'}(\mathbf{r},t)W(\mathbf{r}',\mathbf{r};\mathbf{k}-\mathbf{k}')\phi^*_{v'\mathbf{k}'}(\mathbf{r}',t)\phi_{v\mathbf{k}}(\mathbf{r}',t)d\mathbf{r}'. \tag{7}$$

In Eqs. 5-7 $v(\mathbf{r},\mathbf{r}')$ is the Coulomb potential, $W(\mathbf{r}',\mathbf{r};\mathbf{k}-\mathbf{k}') = \int \epsilon^{-1}(\mathbf{r}',\mathbf{r}'';\mathbf{k}-\mathbf{k}')v(\mathbf{r}'',\mathbf{r})d\mathbf{r}''$ is the statically screened Coulomb interaction, and $W_p = W - v$. We note that, since the Hamiltonian (Eq. 4) depends on the density matrix $\hat{\rho}$, the set of equations 1 for different $\mathbf{k}$ points are coupled; this would be so also for DFT Hamiltonians in the (semi-)local approximation, that depend only on the charge density.

Linearization of Eq. (1) with respect to v_{ext} leads to

$$i\frac{d\hat{\rho}'_{\mathbf{k}}(t)}{dt} = \mathcal{L}\cdot\hat{\rho}'_{\mathbf{k}}(t) + [\hat{v}'_{ext}(t), \hat{\rho}^{\circ}_{\mathbf{k}}], \tag{8}$$

$$\mathcal{L}\cdot\hat{\rho}'_{\mathbf{k}}(t) = \left[\hat{H}^{\circ}_{COHSEX}, \hat{\rho}'_{\mathbf{k}}(t)\right] + [\hat{v}'_H[\hat{\rho}'](t), \hat{\rho}^{\circ}_{\mathbf{k}}] + \left[\hat{\Sigma}'[\hat{\rho}'](t), \hat{\rho}^{\circ}_{\mathbf{k}}\right], \tag{9}$$

where variables with superscript "$^\circ$" represent unperturbed quantities, and those with prime denote linear variations. Within a real space representation, the charge response $\hat{\rho}' = \hat{\rho} - \hat{\rho}^{\circ}$ is given by

$$\rho'(\mathbf{r},\mathbf{r}',t) = \sum_{\mathbf{k}\in BZ} w_{\mathbf{k}}\rho'_{\mathbf{k}}(\mathbf{r},\mathbf{r}',t) = \sum_v \sum_{\mathbf{k}\in BZ} w_{\mathbf{k}}\left[\phi^{\circ}_{v\mathbf{k}}(\mathbf{r})\phi'^{*}_{v\mathbf{k}}(\mathbf{r}',t) + \phi'_{v\mathbf{k}}(\mathbf{r},t)\phi^{\circ *}_{v\mathbf{k}}(\mathbf{r}')\right]. \tag{10}$$

Eq. 10 denotes the linear variation of the density matrix and $\hat{\rho}'_{\mathbf{k}} = \hat{\rho}_{\mathbf{k}} - \hat{\rho}^{\circ}_{\mathbf{k}}$ is the contribution to $\hat{\rho}'$ of the k-point $\mathbf{k}$. We note that $\hat{v}'_H$ and $\hat{\Sigma}'$ depend on the perturbed density matrix $\hat{\rho}'$. In Eq. 9 a non-Hermitian operator $\mathcal{L}$ acting on $\hat{\rho}'_{\mathbf{k}}$ has been defined,

which is known as Liouvillian super-operator[9–11], as its action is defined on a space of operators. By Fourier transforming Eq. 8 into the frequency domain, one obtains

$$(\omega - \mathcal{L}) \cdot \hat{\rho}'_{\mathbf{k}}(\omega) = [\hat{v}'_{ext}(\omega), \hat{\rho}^{\circ}_{\mathbf{k}}] \,. \tag{11}$$

This equation, derived here in the context of the BSE, is formally the same within the density functional perturbation theory (DFPT) formulation of TDDFT (see e.g. Eq. (14) in Ref. 11), but a different definition of the Liouvillian $\mathcal{L}$ is used in the two cases.

The solution of Eq. 11 yields the perturbed density matrix in the frequency domain:

$$\rho'(\mathbf{r},\mathbf{r}',\omega) = \sum_{\mathbf{k}\in BZ} w_{\mathbf{k}} \rho'_{\mathbf{k}}(\mathbf{r},\mathbf{r}',\omega) = \sum_{v} \sum_{\mathbf{k}\in BZ} w_{\mathbf{k}} \left[\phi^{\circ}_{v\mathbf{k}}(\mathbf{r}) \phi'^{*}_{v\mathbf{k}}(\mathbf{r}',-\omega) + \phi'_{v\mathbf{k}}(\mathbf{r},\omega)\phi^{\circ *}_{v\mathbf{k}}(\mathbf{r}')\right] . \tag{12}$$

Eq. 12 shows that $\rho'(\omega)$ is fully determined by the set of the N_v unperturbed occupied states $\phi^{\circ *}_{v\mathbf{k}}$ and by the two sets of N_v perturbed orbitals $\phi'^{*}_{v\mathbf{k}}(\mathbf{r}',-\omega)$ and $\phi'_{v\mathbf{k}}(\mathbf{r},\omega)$, orthogonal to the occupied state subspace. We note that $\rho'(\omega)$, unlike $\rho'(t)$ in Eq. 10, is a non-Hermitian operator. In order to simplify the numerical implementation, we assume time-reversal symmetry holds by imposing $v'_{ext}(\mathbf{r},t) = v'_{ext}(\mathbf{r},-t)$ in Eq. 9. As a consequence $v'_{ext}(\mathbf{r},\omega)$ is a real function and $\phi'_{v-\mathbf{k}}(\mathbf{r},t) = \phi'^{*}_{v\mathbf{k}}(\mathbf{r},-t)$, implying $\phi'_{v-\mathbf{k}}(\mathbf{r},\omega) = \phi'^{*}_{v\mathbf{k}}(\mathbf{r},\omega)$ and $\phi'_{v-\mathbf{k}}(\mathbf{r},-\omega) = \phi'^{*}_{v\mathbf{k}}(\mathbf{r},-\omega)$. Therefore, assuming $v'_{ext}(\mathbf{r},t) = v'_{ext}(\mathbf{r},-t)$ yields a real $\rho'(\omega)$. This assumption does not limit the generality of our approach, since we are interested in computing the macroscopic dielectric function of bulk systems (see Eqs. 13-16 below); the latter is an intrinsic property of the system and does not depend on the specific time or ω dependence of the applied electric field. Furthermore since we can perform the $\mathbf{k} \leftrightarrow -\mathbf{k}$ transformation by a complex conjugate operation, the total number of k-points included in Eqs. 11-12 can be significantly reduced. Details on the time-reversal symmetry operations are given in Appendix A.

The absorption spectrum of a solid is related to the imaginary part of the *macroscopic dielectric function* ε_M defined by the equation (see also[14]):

$$E_{0i}(\omega) = E_i(\omega) + 4\pi P_i(\omega) = \Sigma_j \varepsilon^{ij}_M(\omega) E_j(\omega) \tag{13}$$

where the indexes i and j indicate Cartesian components, $\mathbf{E}_0$ is the applied external electric field, $\mathbf{E}$ is the screened field and $\mathbf{P}$ is the electronic polarization induced by $\mathbf{E}$. In order to compute ε_M, it is convenient to start by setting the value of the screened electric field $\mathbf{E}$[14]. By introducing the potential

$$v'_{ext} = -\mathbf{E}(\omega) \cdot \mathbf{r} \tag{14}$$

in Eq. 11, and expressing the polarization in terms of the density operator,

$$P_i(\omega) = -\frac{1}{V} \sum_{\mathbf{k}\in BZ} w_{\mathbf{k}} Tr(\hat{r}_i \hat{\rho}'_{\mathbf{k}}) = -\frac{1}{V} Tr(\hat{r}_i \hat{\rho}'), \tag{15}$$

from Eq. 13 one has

$$\varepsilon^{ij}_M(\omega) = \delta_{ij} - \frac{4\pi}{V} \sum_{\mathbf{k}\in BZ} w_{\mathbf{k}} \left\langle \hat{r}_i | (\omega - \mathcal{L} + i\eta)^{-1} \cdot [\hat{r}_j, \hat{\rho}^{\circ}_{\mathbf{k}}] \right\rangle , \tag{16}$$

where V is the crystal volume, η is a positive infinitesimal, and we have written the scalar product of two operators A and B as $\langle \hat{A} | \hat{B} \rangle \equiv Tr(\hat{A}^{\dagger} \hat{B})$. As already discussed in the Appendix of Ref.[9], the definition of ϵ_M in Eq. 16 is equivalent to the definition of the BSE macroscopic dielectric function given in Ref.[1] (Eqs. 2.23 and B26). However the formulation of Ref.[9] was so far applicable only to molecules. In addition, the position operator in Eq. 14 is ill defined in periodic boundary conditions; this problem can be overcome within perturbation theory, following Refs.[14,17].

The numerical solution of Eq. 11 and Eq. 16 requires a basis set for $\hat{\rho}'$. From Eq. 12 it follows that only the elements of $\hat{\rho}'$ between unperturbed occupied and empty orbitals are different from zero. The use of those orbitals as a basis set leads to the so called electron-hole (e-h) representation, widely used in the literature to solve the BSE[6–8]. This approach requires the explicit calculation of empty electronic states and convergence with respect to their number has to be carefully checked. By using the projector operators $\hat{Q}_{\mathbf{k}}$ onto the unperturbed empty state subspace, explicit calculations of empty states may be avoided[9]: $\hat{Q}_{\mathbf{k}} = \hat{I} - \hat{P}_{\mathbf{k}} = \hat{I} - \sum_v |\phi^{\circ}_{v\mathbf{k}}\rangle\langle\phi^{\circ}_{v\mathbf{k}}|$, where $\hat{P}_{\mathbf{k}}$ is the projector onto the occupied state subspace for a fixed $\mathbf{k}$ in the first BZ and $\hat{I}$ is the identity operator. The evaluation of $\hat{Q}_{\mathbf{k}}$ does not require the explicit calculation of empty states. Since Bloch states corresponding to different k-points are orthogonal, the projection can be preformed independently for each k-point. Within this formalism a generic operator $\hat{A}$ can be represented by a set of $2\times\mathrm{N}_v\times\mathrm{N}_{\mathbf{k}}$ orbitals that are defined in the following way:

$$|a_{v\mathbf{k}}\rangle = \hat{Q}_{\mathbf{k}} \hat{A} |\phi^{\circ}_{v\mathbf{k}}\rangle, \tag{17}$$

$$\langle b_{v\mathbf{k}}| = \langle \phi^{\circ}_{v\mathbf{k}}| \hat{A} \hat{Q}_{\mathbf{k}}, \tag{18}$$

where the index v runs from 1 to the number of occupied bands N_v, while $\mathbf{k}$ is a point of the discrete mesh used to perform the integral in the first BZ. If $\hat{A} = \hat{\rho}'$ we have $a_{v\mathbf{k}}(\mathbf{r}) = \phi'_{v\mathbf{k}}(\mathbf{r},\omega)$ and $b_{v\mathbf{k}}(\mathbf{r}) = \phi'_{v\mathbf{k}}(\mathbf{r},-\omega)$. Within this representation the operator $\mathcal{L}$ takes the form:

$$\mathcal{L} = \begin{pmatrix} \mathcal{D} + 2\mathcal{K}^{1x} - \mathcal{K}^{1d} & 2\mathcal{K}^{2x} - \mathcal{K}^{2d} \\ -2\mathcal{K}^{2x} + \mathcal{K}^{2d} & -\mathcal{D} - 2\mathcal{K}^{1x} + \mathcal{K}^{1d} \end{pmatrix}, \tag{19}$$

where $\mathcal{D}$, the exchange terms $\mathcal{K}^{1x}$ and $\mathcal{K}^{2x}$ and the direct terms $\mathcal{K}^{1d}$ and $\mathcal{K}^{2d}$ are defined as:

$$\sum_{v'} \sum_{\mathbf{k}' \in BZ} \mathcal{D}_{v\mathbf{k},v'\mathbf{k}'} \, |a_{v'\mathbf{k}'}\rangle = \sum_{v'} \sum_{\mathbf{k}' \in BZ} (\hat{H}^{\circ}_{COHSEX} - \epsilon_{v'\mathbf{k}'}) \, \delta_{vv'} \, \delta_{\mathbf{k}\mathbf{k}'} |a_{v'\mathbf{k}'}\rangle, \tag{20}$$

$$\sum_{v'} \sum_{\mathbf{k}' \in BZ} \mathcal{K}^{1x}_{v\mathbf{k},v'\mathbf{k}'} \, |a_{v'\mathbf{k}'}\rangle = \sum_{v'} \sum_{\mathbf{k}' \in BZ} w_{\mathbf{k}'} \hat{Q}_{\mathbf{k}} \left(\int \frac{1}{|\mathbf{r} - \mathbf{r}'|} \phi^{\circ *}_{v'\mathbf{k}'}(\mathbf{r}') a_{v'\mathbf{k}'}(\mathbf{r}') d\mathbf{r}' \right) |\phi^{\circ}_{v\mathbf{k}}\rangle, \tag{21}$$

$$\sum_{v'} \sum_{\mathbf{k}' \in BZ} \mathcal{K}^{2x}_{v\mathbf{k},v'\mathbf{k}'} \, |b_{v'\mathbf{k}'}\rangle = \sum_{v'} \sum_{\mathbf{k}' \in BZ} w_{\mathbf{k}'} \hat{Q}_{\mathbf{k}} \left(\int \frac{1}{|\mathbf{r} - \mathbf{r}'|} b^{*}_{v'\mathbf{k}'}(\mathbf{r}') \phi^{\circ}_{v'\mathbf{k}'}(\mathbf{r}') d\mathbf{r}' \right) |\phi^{\circ}_{v\mathbf{k}}\rangle, \tag{22}$$

$$\sum_{v'} \sum_{\mathbf{k}' \in BZ} \mathcal{K}^{1d}_{v\mathbf{k},v'\mathbf{k}'} \, |a_{v'\mathbf{k}'}\rangle = \sum_{v'} \sum_{\mathbf{k}' \in BZ} w_{\mathbf{k}'} \hat{Q}_{\mathbf{k}} \left(\int W(\mathbf{r},\mathbf{r}';\mathbf{k}-\mathbf{k}') \phi^{\circ *}_{v'\mathbf{k}'}(\mathbf{r}') \phi^{\circ}_{v\mathbf{k}}(\mathbf{r}') d\mathbf{r}' \right) |a_{v'\mathbf{k}'}\rangle, \tag{23}$$

$$\sum_{v'} \sum_{\mathbf{k}' \in BZ} \mathcal{K}^{2d}_{v\mathbf{k},v'\mathbf{k}'} \, |b_{v'\mathbf{k}'}\rangle = \sum_{v'} \sum_{\mathbf{k}' \in BZ} w_{\mathbf{k}'} \hat{Q}_{\mathbf{k}} \left(\int W(\mathbf{r},\mathbf{r}';\mathbf{k}-\mathbf{k}') b^{*}_{v'\mathbf{k}'}(\mathbf{r}') \phi^{\circ}_{v\mathbf{k}}(\mathbf{r}') d\mathbf{r}' \right) |\phi^{\circ}_{v'\mathbf{k}'}\rangle. \tag{24}$$

The operator $\mathcal{D}$ describes bare single particle ground-state excitations, the $\mathcal{K}^{1x}$ and $\mathcal{K}^{2x}$ terms include so-called local field effects and the $\mathcal{K}^{1d}$ and $\mathcal{K}^{2d}$ terms describe electron-hole interactions. The integrals entering the definition of $\mathcal{K}^{1d}$ and $\mathcal{K}^{2d}$ include divergent terms in reciprocal space; in our implementation these divergences are integrated by using the method proposed in Refs.[18,19].

The formalism described here to solve the BSE is equivalent to a time-dependent COHSEX within linear response; the COHSEX self-energy enters both in the definition of the bare independent quasi-particle (QP) ground-state excitations in $\mathcal{D}$ and in the $\mathcal{K}^{1d}$ and $\mathcal{K}^{2d}$ components of the kernel. In the linearization procedure used in Eqs. 8-9, the dependence of W (which enters Σ_{COHSEX}) on the density matrix is neglected[20]; this implies that only the linearized Σ_{SEX} contributes to $\mathcal{K}^{1d}$ and $\mathcal{K}^{2d}$. The COHSEX approximation is known to overestimate quasi-particle gaps[21], and single particle states and eigenvalues obtained within the GW approximation are usually preferred as starting points for BSE calculations. Within our current implementation $\hat{H}^{\circ}_{QP}$ ($\hat{H}^{\circ}_{COHSEX}$) is approximated either by the Kohn-Sham (KS) Hamiltonian whose gap is corrected by the use of a scissor shift Δ ($\hat{H}^{\circ}_{QP} = \hat{H}^{\circ}_{LDA} + \Delta\hat{Q}_{\mathbf{k}}$) or by including several GW corrected eigenvalues using Eqs. $24-25$ in Ref.[9]; the scissor approximation is accurate for the s-p bonded solids considered in this work[22]. The introduction of a more general scheme to include quasi-particle corrections within our formulation of the BSE will be the subject of future work. For example, the use in Eq. 20 of the enhanced COHSEX approximation presented in Ref.[23] may yield quasi-particle corrections of accuracy similar to that of the GW approximation, in a way fully consistent with our formulation.

The evaluation of the integrals defined by Eqs. 23-24 is the most expensive part in a BSE calculation. We note that the number of orbitals involved in the definition of $\mathcal{K}^{1d}$ and $\mathcal{K}^{2d}$ is equal to the number of occupied states. Hence the scalability of our approach is the same as that of a ground state Hartree-Fock calculation (assuming $W = v$ for simplicity; the scalability of the calculation of the dielectric matrix is discussed in detail in Ref.[12]). Specifically, in a plane-wave (PW) implementation the evaluation of $\mathcal{K}^{1d}$ and $\mathcal{K}^{2d}$ scales as $\alpha[N_v^2 \times N_{\mathbf{k}}^2 \times N_{PW} \times \log N_{PW}]$, where N_{PW} is the size of the plane-wave basis set and α is constant with respect to system size; this is exactly the same scaling as that of calculations of the Hartree-Fock exact-exchange; as shown in the next section the computational complexity can be further decreased to $\alpha[N_v^2 \times N_{\mathbf{k}} \times N_{\mathbf{k}_I} \times N_{PW} \times \log N_{PW}]$, where $N_{\mathbf{k}_I}$ is the number of k-points in the irreducible Brillouin zone, by exploiting the symmetry operations of the system point group. In general the constant (or pre-factor) α of a BSE calculation is much larger than that of a ground state Hartree-Fock calculation. For example for the systems studied in this work, a number of Lanczos iterations between 1000 and 2000 is necessary to achieve convergence and for each iteration four operations are performed, with the same complexity of Hartree-Fock exact-exchange calculations (only one of such operations is required within the Tamm-Dancoff approximation). Within a electron-hole approach, the evaluation of $\mathcal{K}^{1d}$ and $\mathcal{K}^{2d}$ scales as $[N_v \times N_c \times N_{\mathbf{k}}^2 \times N_{PW} \times \log N_{PW}]$. Since in general N_c is much larger than N_v, the approach presented in this work is more efficient than an electron-hole approach and increasingly so for large systems. Within a matrix representation, the dimension of $\mathcal{L}$ (Eq. 19) is $2 \times N_v \times N_c \times N_{\mathbf{k}}$ in an e-h approach. Only in cases where N_c and $N_{\mathbf{k}}$ can be chosen small enough, the matrix $\mathcal{L}$ can be built explicitly and kept in memory for subsequent use (such as, i.e., the calculation of the dielectric tensor using the Lanczos algorithm). Storing $\mathcal{L}$ clearly allows for a large decrease in the pre-factor α of e-h BSE calculations, with respect to those presented here. However explicit calculation and storage of $\mathcal{L}$ are possible only for relatively small systems, as the required memory becomes rapidly unaffordable for large values of N_c

and $N_{\mathbf{k}}$. Within the density matrix perturbation theory approach of this work, the dimension of $\mathcal{L}$ is $2 \times N_v \times N_{PW} \times N_{\mathbf{k}}$; if one chooses N_c to be the total number of conduction states, since $N_c \gg N_v$ and $N_{PW} = N_c + N_v \approx N_c$, the matrices representing $\mathcal{L}$ in the density matrix perturbation theory approach and in the e-h approach have similar dimensions[15]. N_{PW} is usually a large number, and thus within our method the matrix $\mathcal{L}$ is never built explicitly. Our approach is instead based on iterative calculations, where the application of $\mathcal{L}$ to a generic vector is performed by taking advantage of procedures analogous to those used in applying the Hamiltonian to wavefunctions in ground state calculations.

In the evaluation of $\mathcal{K}^{1d}$ and $\mathcal{K}^{2d}$, one needs to evaluate the inverse dielectric matrix ϵ^{-1} entering the definition of the screened Coulomb interaction $W(\mathbf{r}', \mathbf{r}; \mathbf{q}) = \int \epsilon^{-1}(\mathbf{r}', \mathbf{r}''; \mathbf{q}) v(\mathbf{r}'', \mathbf{r}) d\mathbf{r}''$ (where $\mathbf{q}$ is a generic wave vector). Also in this case the explicit calculation of empty electronic states can be avoided by using DFPT. In particular, following Refs. [12,13], we use an eigenvalue decomposition of the symmetrized dielectric matrix[24] $\widetilde{\epsilon}$ in the random-phase approximation (RPA), and an iterative algorithm to obtain eigenvalues and eigenvectors: such algorithm involves the evaluation of the action of $\widetilde{\epsilon}$ on trial potentials. Finally no inversion of the dielectric matrix is necessary as a spectral decomposition of $\widetilde{\epsilon}^{-1}$ is easily obtained from the eigenvalues (λ_i) and eigenvectors ($\widetilde{\mathbf{v}}_i$) of $\widetilde{\epsilon}$:

$$\widetilde{\epsilon}^{-1}(\mathbf{q}) = \hat{I} + \sum_{i=1}^{N} |\widetilde{\mathbf{v}}_i(\mathbf{q})\rangle (\lambda_i^{-1}(\mathbf{q}) - 1) \langle \widetilde{\mathbf{v}}_i(\mathbf{q})|, \tag{25}$$

As shown in Ref.[9] and in Sec. IV below, convergence of computed spectra can be achieved with a small number N of eigenpairs included in Eq. 25. Indeed it has been shown that the eigenvalues λ_i are always greater than or equal to 1[24] and that for a variety of systems $(\lambda_i^{-1} - 1)$ decays rapidly to zero, as the eigenvalue index increases[12,13].

III. USE OF SYMMETRIES IN THE SOLUTION OF THE BETHE-SALPETER EQUATION

As shown in the previous section, the solution of the BSE for crystalline materials (and in general for periodic systems) involves the evaluation of integrals over a grid in the first Brillouin zone. Our implementation exploits the symmetry of the system to reduce the computational time and the memory requirements of the calculations. In a crystal the most general symmetry operation is given by a combination of a rotation R and a fractional translation $\mathbf{f}$ (denoted by $\{R|\mathbf{f}\}$). The set of symmetry operations $\{R|\mathbf{f}\}$ constitute the space group of the crystal. By using rotations R, we can express a generic point in the BZ as $\mathbf{k} = R\mathbf{k}_I$, where $\mathbf{k}_I$ belongs to the irreducible BZ (IBZ). The unperturbed Bloch wavefunctions satisfy the following equation[25]:

$$\phi^{\circ}_{v\mathbf{k}}(\mathbf{r}) = \phi^{\circ}_{vR\mathbf{k}_I}(\mathbf{r}) = \phi^{\circ}_{v\mathbf{k}_I}(R^{-1}\mathbf{r} - \mathbf{f}). \tag{26}$$

The perturbed orbitals implicitly depend on the direction of the electric field (Eq. 14). For this reason they satisfy the relationship:

$$\phi'^{i}_{v\mathbf{k}}(\mathbf{r}, \omega) = \phi'^{i}_{vR\mathbf{k}_I}(\mathbf{r}, \omega) = \sum_j R_{ij} \phi'^{j}_{v\mathbf{k}_I}(R^{-1}\mathbf{r} - \mathbf{f}, \omega) \tag{27}$$

where i and j indicate Cartesian coordinates; the same relationship holds for the $\phi'^{*}_{v\mathbf{k}}(\mathbf{r}, -\omega)$ perturbed orbitals. These properties can be used to improve the efficiency of the numerical solution of the equations described in the previous section. We first consider the calculation of P_i in Eq. 15. From the definition of $\hat{\rho}'(\omega)$ in Eq. 12 we have

$$P_{ij}(\omega) = -\frac{1}{V} \sum_{\mathbf{k} \in BZ} w_{\mathbf{k}} Tr(\hat{r}_i \hat{\rho}'^{j}_{\mathbf{k}}) = -\frac{1}{V} \int r_i \rho'^{j}(\mathbf{r}, \omega) d\mathbf{r}, \tag{28}$$

where we have emphasized the dependence of P_i and $\hat{\rho}'_{\mathbf{k}}$ on the direction of the electric field, corresponding to the j-th Cartesian coordinate. By defining

$$\varrho'^{j}(\mathbf{r}, \omega) = \sum_{\mathbf{k_I} \in IBZ} w_{\mathbf{k_I}} \rho'^{j}_{\mathbf{k_I}}(\mathbf{r}, \omega) \tag{29}$$

from Eqs. 26-27 and Eq. 12, we have

$$\rho'^{j}(\mathbf{r}, \omega) = \frac{1}{N_S} \sum_R \sum_l R_{jl} \varrho'^{l}(R^{-1}\mathbf{r} - \mathbf{f}, \omega) \tag{30}$$

where N_S indicates the number of symmetry operations of the space group of the system; finally one has:

$$\begin{aligned} P_{ij} &= -\frac{1}{V} \frac{1}{N_S} \sum_R \sum_l R_{jl} \int r_i \varrho'^{l}(R^{-1}\mathbf{r} - \mathbf{f}, \omega) d\mathbf{r} \\ &= -\frac{1}{V} \frac{1}{N_S} \sum_R \sum_{l,m} R_{im} R_{jl} \int r_m \varrho'^{l}(\mathbf{r}, \omega) d\mathbf{r}. \end{aligned} \tag{31}$$

The set of Eqs. 29-31 shows that the perturbed density matrix $\hat{\rho}'$ (and consequently the macroscopic dielectric function) can be computed by solving Eq. 11 only for the k-points in the irreducible Brillouin zone instead of the full Brillouin zone. Symmetry operations can be further exploited in the calculation of the $\mathcal{K}^{1x}$ and $\mathcal{K}^{2x}$ components of the kernel defined in Eqs. 21-22. To this end in Eq. 21 we define:

$$n'^j(\mathbf{r}') = \sum_{v'} \sum_{\mathbf{k}' \in BZ} w_{\mathbf{k}'} \phi^{\circ *}_{v'\mathbf{k}'}(\mathbf{r}') a^j_{v'\mathbf{k}'}(\mathbf{r}') = \sum_{\mathbf{k}' \in BZ} w_{\mathbf{k}'} n'^j_{\mathbf{k}'}(\mathbf{r}'), \tag{32}$$

where the orbitals $a^j_{v\mathbf{k}}(\mathbf{r})$ satisfy Eq. 27 (where for simplicity we have omitted the implicit dependence on the j-th Cartesian coordinate). Likewise in Eq. 29, we define

$$\widetilde{n}'^j(\mathbf{r}') = \sum_{\mathbf{k_I} \in IBZ} w_{\mathbf{k_I}} n'^j_{\mathbf{k_I}}(\mathbf{r}') \tag{33}$$

and finally we have

$$n'^j(\mathbf{r}') = \frac{1}{N_S} \sum_R \sum_l R_{jl} \widetilde{n}'^l(R^{-1}\mathbf{r}' - \mathbf{f}). \tag{34}$$

Eq. 33 implies that, in order to evaluate the term in parentheses in Eq. 21 (and in Eq. 22), it is necessary to consider only the orbitals corresponding to $\mathbf{k}'$ points inside the irreducible BZ. Such simplification cannot be exploited in a straightforward manner for the calculation of $\mathcal{K}^{1d}$ and $\mathcal{K}^{2d}$ as defined in Eqs. 23-24, where one needs to sum $\mathbf{k}'$ over the full BZ.

In order to calculate $\rho'^j(\mathbf{r}, \omega)$, the linear system of Eq. 11 is iteratively solved using the non-Hermitian Lanczos algorithm introduced in Ref.[11]. To apply the required symmetrization operations (i.e. Eq. 34), three simultaneous iterative chains are performed at the same time, corresponding to the three directions of the perturbing electric field.

IV. APPLICATIONS TO BULK SILICON, CARBON DIAMOND AND SILICON CARBIDE

The formalism presented in the previous sections has been implemented in the framework of the Quantum Espresso (QE) package, that uses plane-waves as a basis set and pseudopotentials[26]. The quasi-particle Hamiltonian $\hat{H}^\circ$ in Eq. 20 is approximated by $\hat{H}_{KS} + \Delta\hat{Q}_{\mathbf{k}}$, where $\hat{H}_{KS}$ is the Kohn-Sham (KS) Hamiltonian and Δ is the difference between the quasi-particle gap and the KS gap (scissor approximation). From quasi-particle (QP) calculations at the GW level of theory[16] it is known that the scissor approximation is accurate for the description of the band structure of several sp-bonded bulk systems[22].

We computed the absorption spectra of solids as the imaginary part of the macroscopic dielectric function ε_M (Eq. 16). In general ε_M is a tensor but in the specific cases studied here this tensor is diagonal and the diagonal elements all have the same value.

We first discuss the absorption spectrum of bulk silicon. The ground state calculation has been performed using the local density approximation (LDA) in the Perdew-Zunger[27] parametrization and the pseudopotential was taken from the Quantum Espresso library[28]. We used a lattice constant optimized at the LDA level of theory (10.20 a_0), as given in Ref.[29]. The value of the scissor shift Δ is determined as the difference of the experimental value of the minimum direct QP gap at the Γ point (3.4 eV)[30] and the LDA gap at the same point (2.57 eV). The use of a computed G_0W_0 quasi-particle gap would not significantly affect our results, since the G_0W_0 approximation reproduces the experimental value within 0.1 eV[22]. A cutoff of 18 Ry was used to expand the ground-state wavefunctions as well as the dielectric matrix (in Eq. 25); all the empty bands described by this cut-off are implicitly included in our calculation, corresponding to at least 328 empty bands per k-point. In Refs.[6,7], as few as 4 conduction states were considered sufficient to reasonably converge the spectrum of bulk silicon. However, even in this case, our approach has a few advantages over the traditional e-h approach: the convergence with respect to the number of empty states does not need to be tested; the number of perturbed orbitals included in our calculations is equal to N_v(=4); due to the large amount of e-h pairs included implicitly in our approach the spectrum can be computed up to high energy and the validity of the f-sum rule can be easily verified (see below).

As shown in Ref.[31] the convergence of the static macroscopic dielectric constant (head of the dielectric matrix) is rather slow with respect to the k-points included in the first BZ. In order to integrate the BSE we use Monkhorst-Pack (M-P) grids of special k-points as implemented in QE[32,33]. As shown in the early work of Benedict *et al.*[8], in order to improve the convergence of computed spectra it is useful to shift the grid from the origin (Γ point). In the QE implementation, automatically generated k-point grids centered at Γ may be shifted by $\left(\frac{1}{2n}\mathbf{b}_1 + \frac{1}{2n}\mathbf{b}_2 + \frac{1}{2n}\mathbf{b}_3\right)$, where n is the grid dimension and $\mathbf{b}_1$, $\mathbf{b}_2$ and $\mathbf{b}_3$ are reciprocal lattice primitive vectors. Since in the face-centered cubic lattice after such shift the k-point grid does not have the full symmetry of the crystal, additional points are generated, leading to a mesh with four times the number of k-points as in the original grid. This fact can be understood in the simple case of a single k-point $1 \times 1 \times 1$ mesh shifted in $\left(\frac{1}{2}\mathbf{b}_1 + \frac{1}{2}\mathbf{b}_2 + \frac{1}{2}\mathbf{b}_3\right)$.

By applying all the symmetry operations (48 for the systems considered in this work) we can generate additional k-points $\frac{1}{2}\mathbf{b}_1$, $\frac{1}{2}\mathbf{b}_2$, $\frac{1}{2}\mathbf{b}_3$ equivalent by symmetry. This leads to a mesh with four times the k-points as the original $1 \times 1 \times 1$ mesh. Of course only the k-point $\left(\frac{1}{2}\mathbf{b}_1 + \frac{1}{2}\mathbf{b}_2 + \frac{1}{2}\mathbf{b}_3\right)$ is included in the IBZ and this property is exploited to accelerate the calculations, as discussed in Sec. III. If the single k-point is shifted by a random vector in the BZ, the application of the symmetry operations may lead up to 48 different k-points in the full BZ (this is the number of symmetry operations of the point group of the diamond lattice). Similar arguments can be applied to the case of a k-point mesh of larger dimensions. The convergence with respect to the dimension of the grid is discussed below.

In order to test the computational parameters and approximations entering the solution of the BSE, we have first performed calculations for Si with a $4\times4\times4$ mesh with the origin shifted by $\left(\frac{1}{8}\mathbf{b}_1 + \frac{1}{8}\mathbf{b}_2 + \frac{1}{8}\mathbf{b}_3\right)$. This grid is then symmetrized, leading to 256 k-points in the full BZ and 10 in the IBZ. This mesh is sufficient to obtain accurate ground state properties but does not yield converged results for absorption spectra; nevertheless it is sufficiently accurate for the purpose of testing additional numerical parameters and approximations involved in the solution of the BSE. In Fig. 1 we show the convergence of the absorption spectrum of bulk silicon as a function of the number of eigenvalues and eigenvectors used in Eq. 25. The convergence is rapid and no difference is present between the spectra obtained using 16 and 48 eigenvalues. We note that the dimension of the full matrix is 2733, that is much bigger than the small number of eigenpotentials used here for its representation. In Fig. 2 we compare results obtained with and without the Tamm-Dancoff approximation (TDA). Minor differences are observed only in the high energy part of the spectrum. We have also computed the f-sum rule for these spectra and found that the full BSE fulfills 97% of the f-sum rule while the TDA spectrum yields 107%. The TDA appears to be reliable for the optical properties of bulk systems, as widely accepted since the early use of the BSE[7]. However the TDA may break down for the optical spectra of molecules and nanostructures[9,34] and for the electron energy loss spectra of bulk systems[35]. In the following, calculations on larger k-point grids are carried out within the TDA approximation.

We now consider the convergence of the spectrum of bulk silicon as a function of the dimension of the k-point grid used in the calculations. In Fig. 3 we show the results for three different Monkhorst-Pack (M-P) grids[32] of dimension $n \times n \times n$ with $n = 8, 10,$ and 12, respectively, and we compare them with the experimental spectrum[36]. In order to improve the convergence, the origin of those grids is shifted by $\left(\frac{1}{2n}\mathbf{b}_1 + \frac{1}{2n}\mathbf{b}_2 + \frac{1}{2n}\mathbf{b}_3\right)$. After symmetrization the total number of k-points in the grid is $4 \times n \times n \times n$. Our calculations give accurate results for the position and intensity of the two main peaks, compared to experiment, with an error of at most 0.12 eV for the first (E_1) transition. However in the computed spectra we obtain a weak additional peak between the two main transitions which has a strong dependence on the k-point mesh used in the calculation. This extra peak was already present in some of the earlier BSE calculations of the optical spectrum of bulk silicon[6,7] and in recent publications[37], as shown in Fig. 4. When the same k-point mesh is used, our approach reproduces the same result of a well converged electron-hole calculation (see panel b of Fig. 4).

Since the early applications of the BSE to the calculation of spectra of bulk systems, it was suggested that the use of M-P grids was likely responsible for the appearance of spurious peaks in the spectra[38]. It was also suggested that the use of grids shifted off the high symmetry directions[8] or randomly distributed k-points may help avoid the appearance of spurious spectral features. For example in Ref.[38] the example of an independent particle spectrum computed with 400000 k-points was presented, showing improved accuracy. However such a large mesh is not affordable in the solution of the BSE for realistic solids. For the sake of completeness, in this work we have also considered the use of a k-point grid off symmetry, obtained by shifting the origin of a regular grid at $\frac{1}{64}\mathbf{b}_1 + \frac{1}{32}\mathbf{b}_2 + \frac{3}{64}\mathbf{b}_3$, as suggested in Refs[8,38]; in this case the grid is not symmetrized and the formalism described in Sec. III to accelerate the calculations cannot be applied (only the time-reversal symmetry is used, as explained in Appendix A). The results are shown in Fig. 5 for some of the components of the dielectric tensor. Since the grid does not have the full symmetry of the crystal, the diagonal components of ε_M are different from each other, and the off-diagonal components of the tensor are different from zero. In Ref.[8] the perturbation was applied along the $(1, 1, 1)$ direction, amounting to an average of all the components of the tensor. This average eliminates the spurious peaks, which, however, are still present on the xx and yy diagonal components of the tensor (see Fig. 5). In this work, we have not considered random k-points in the integration of the BSE. In the literature, the BSE spectrum of silicon has already been computed using 1000 k-points randomly distributed over the BZ, finding a shoulder instead of a peak between the two main transitions (see Fig.2 of Ref.[39]). Since a random distribution of k-points does not have the lattice symmetry, an effect analogous to the one shown in Fig. 5 might occur also in this case, especially for a small set of k-points. We note that a systematic test of the convergence of random distributions of k points or grids shifted off-symmetry can not take advantage of the symmetry to simplify the calculations and would become rapidly impractical when increasing the size of the sampling.

As a further application of our technique we have computed the absorption spectrum of carbon diamond. Also in this case the ground state calculation was performed using the local density approximation (LDA) and the pseudopotentials were taken from the Quantum Espresso library[28]. The lattice parameter was set to the experimental value of 6.74 a_0[40]. A cutoff of 40 Ry was used to expand the wavefunctions and more than 300 empty band are implicitly included in our calculation. The value of the scissor shift Δ is obtained as the difference between the value of the experimental minimum direct gap (7.3 eV)[41] and the LDA minimum direct gap (5.66 eV). As shown in Ref.[22] the G_0W_0 quasi-particle and the experimental gap differ by 0.2 eV. As suggested in Ref.[8] a 6.4% stretch of the valence band was applied, to correct for the underestimate of the valence band width given by the LDA.

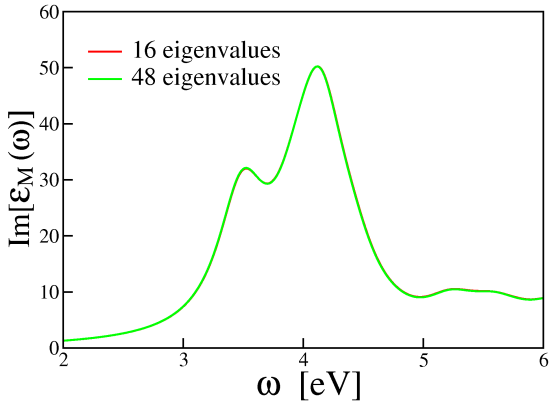

Figure 1: Absorption spectrum of bulk silicon computed as a function of the number of eigenvalues and eigenvectors used in the spectral decomposition of the dielectric matrix (Eq. 25). A mesh of 256 k-points in the BZ corresponding to 10 k-points in the IBZ has been used. A Lorentzian broadening of 0.24 eV was added to the curves.

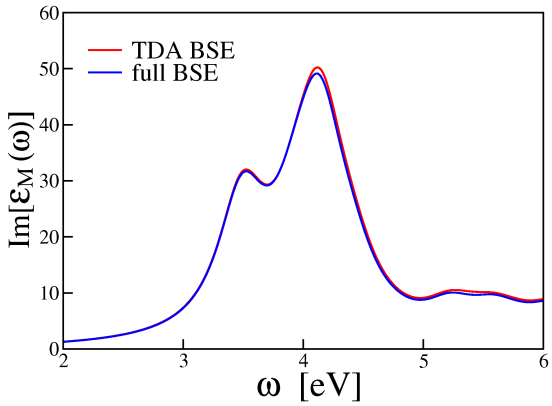

Figure 2: Absorption spectrum of bulk silicon computed with and without the Tamm-Dancoff approximation (TDA). A mesh of 256 k-points in the BZ corresponding to 10 k-points in the IBZ has been used. A Lorentzian broadening of 0.24 eV was added to the curves. We used 16 eigenvalues in Eq. 25 (see Fig. 1).

We tested the convergence of our results with respect to the number of eigenpairs included in Eq. 25 and the accuracy of the Tamm-Dancoff approximation. The conclusions are similar to the case of bulk silicon. In Fig. 6 we show the results for the calculated absorption spectrum of carbon diamond for two different k-point grids and we compare them with the experimental curve (from Ref.[42]). In this case the convergence with respect to the dimension of the k-point grid is faster than for bulk silicon; however, following Ref.[43] a larger Lorentzian broadening than in bulk Si was used for the computed spectrum (0.57 eV), which overall has less features than that of Si. The comparison with the experimental data is satisfactory, with a shift in the main peak of about 0.1 eV.

As a final example we consider the absorption spectrum of silicon carbide in the zincblende structure. The calculation was performed in the local density approximation with the lattice parameter set to the experimental value of 8.24 a_0[40]. A cutoff of 40 Ry was used to expand the wavefunctions, corresponding to the implicit inclusion of more than 580 empty states. The value of the scissor shift is obtained as the difference between the experimental gap of 2.39 eV[40] and the LDA gap of 1.30 eV. In Fig. 7 we show the BSE spectrum computed for a $8 \times 8 \times 8$ shifted k-point mesh and the experimental curve from Ref.[44]. Overall the agreement between theory and experiment is good and the main peak position is reproduced with an error of about 0.15 eV. If a Lorentzian broadening of 0.57 is used, as in the case of diamond, a good agreement between the computed and experimental intensity is found, but the first shoulder of the experimental spectrum is not visible. This shoulder becomes detectable in the spectrum computed using a 0.27 eV broadening. In this case the intensity of the main peak is overestimated; overall our computed spectra are similar to previous results in the literature[39,45].

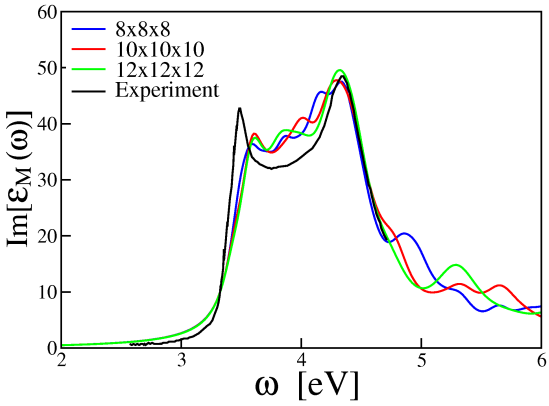

Figure 3: Absorption spectrum of bulk silicon computed with different Monkhorst-Pack k-point grids, compared to the experimental results[36]. A Lorentzian broadening of 0.11 eV has been added to the computed curves.

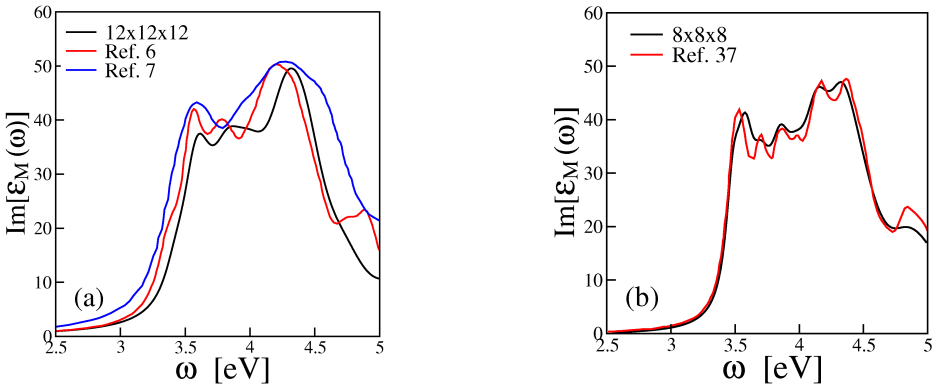

Figure 4: (a) Comparison of the bulk silicon spectrum (computed with a $12 \times 12 \times 12$ shifted k-grid) with some of the early BSE calculations (Ref.[6] and Ref.[7]). In Ref.[6] a grid containing 2048 k-points in the BZ was used while in Ref.[7] a 32 k-point grid was extrapolated up to 500 k-points. (b) Comparison of the bulk silicon spectrum computed using an $8 \times 8 \times 8$ shifted k-grid using our method and the electron-hole implementation of the Yambo code[37]; in this case an energy dependent broadening was used in order to compare with Ref.[37] (in the energy range shown in the figure the broadening increases linearly from 0.02 eV to 0.15 eV as a function of ω).

V. CONCLUSIONS

In this work we have presented the extension to periodic systems of the density matrix perturbation theory formalism[9] for the calculation of optical absorption spectra. Within this approach the explicit calculation of empty electronic states and the storage and inversion of the dielectric matrix for the calculation of the screened Coulomb interaction are avoided. The use of both spatial and time-reversal symmetries leads to a significant reduction of the computational workload. As a proof of principle, we have applied our approach to the calculation of the optical absorption spectra of bulk silicon, carbon diamond and silicon carbide. The convergence of numerical parameters, such as the dimension of the k-point grid and the number of eigenpairs used to expand the dielectric screening, have been carefully discussed. The accuracy of the Tamm-Dancoff approximation for bulk systems has been confirmed by the explicit calculation of absorption spectra and sum rules. Our results exhibit good agreement with previously published data[6–8] and with experimental spectra[36,42].

This work was supported by NSF CHE-0802907 grant and DOE BES-FG02-06ER46262 grant and computer time was provided by NERSC and Teragrid under grant numbers TG-ASC090004 and TG-MCA06N063. We gratefully acknowledge many useful discussions with Deyu Lu, Andrea Dal Corso and Stefano Baroni.

Appendix A: Time-reversal symmetry

In order to simplify the implementation described in Sec. II, it is useful to exploit the time-reversal symmetry in the solution of the Bethe-Salpeter equation, which consists in assuming $v_{ext}(\mathbf{r}, t) = v_{ext}(\mathbf{r}, -t)$ in Eq. 4. The use of this symmetry yields a real perturbed density matrix in the frequency domain (Eq. 12), and the actual number of k-points needed in Eqs. 11-12 is

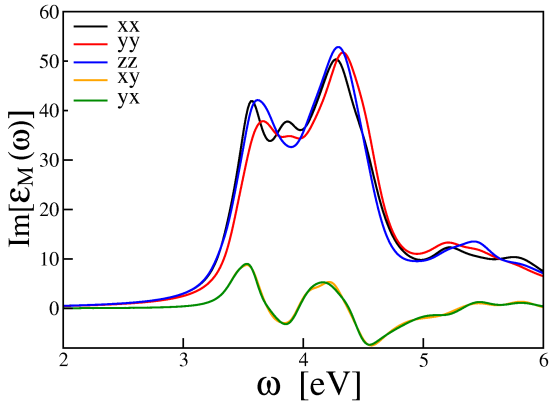

Figure 5: Absorption spectrum of bulk silicon computed with the nonsymmetric k-point mesh proposed in Ref.[8]. A Lorentzian broadening of 0.11 eV has been added to the curves. The different components of ε_M are represented by different colors.

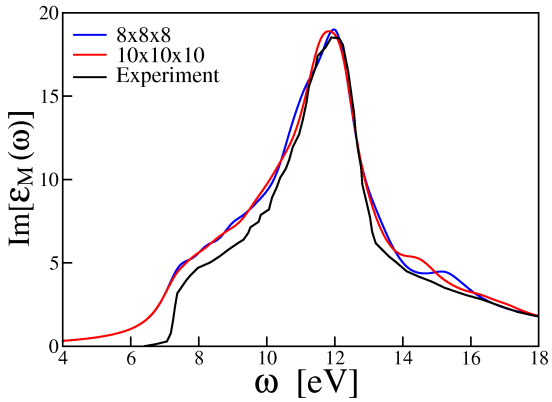

Figure 6: Absorption spectrum of carbon diamond as computed with different Monkhorst-Pack k-point grids, compared to the experimental results from Ref.[42]. We used 16 eigenvalues in Eq. 25. A Lorentzian broadening of 0.57 eV has been added to the computed curves.

decrease by about 50%. For the sake of simplicity we will first illustrate the time-reversal symmetry result for a generic real non-local Hamiltonian which satisfies the property $\hat{H}(\mathbf{r},\mathbf{r}',t) = \hat{H}(\mathbf{r},\mathbf{r}',-t)$. We consider the corresponding time-dependent Schrödinger equation

$$i\frac{d\phi_{v\mathbf{k}}(\mathbf{r},t)}{dt} = \int \hat{H}(\mathbf{r},\mathbf{r}',t)\phi_{v\mathbf{k}}(\mathbf{r}',t)d\mathbf{r}'. \tag{A1}$$

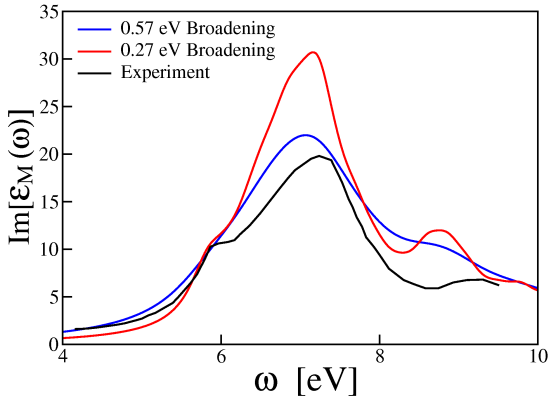

Figure 7: Absorption spectrum of silicon carbide as computed with an $8 \times 8 \times 8$ shifted Monkhorst-Pack k-point grid compared to the experimental results from Ref.[44]. The results are shown for two different values of the Lorentzian broadening.

By time inversion one has:

$$-i\frac{d\phi_{v\mathbf{k}}(\mathbf{r},-t)}{dt} = \int \hat{H}(\mathbf{r},\mathbf{r}',t)\phi_{v\mathbf{k}}(\mathbf{r},-t)d\mathbf{r}' \tag{A2}$$

and the complex conjugate of this equation is:

$$i\frac{d\phi^*_{v\mathbf{k}}(\mathbf{r},-t)}{dt} = \int \hat{H}(\mathbf{r},\mathbf{r}',t)\phi^*_{v\mathbf{k}}(\mathbf{r},-t)d\mathbf{r}'. \tag{A3}$$

By comparing Eq. A3 with the time-dependent Schrödinger equation corresponding to $-\mathbf{k}$

$$i\frac{d\phi_{v-\mathbf{k}}(\mathbf{r},t)}{dt} = \int \hat{H}(\mathbf{r},\mathbf{r}',t)\phi_{v-\mathbf{k}}(\mathbf{r},t)d\mathbf{r}' \tag{A4}$$

we have that

$$\phi_{v-\mathbf{k}}(\mathbf{r},t) = \phi^*_{v\mathbf{k}}(\mathbf{r},-t); \tag{A5}$$

by Fourier transforming Eq. A5 one has:

$$\phi_{v-\mathbf{k}}(\mathbf{r},\omega) = \phi^*_{v\mathbf{k}}(\mathbf{r},\omega). \tag{A6}$$

It is important to note that $\hat{H}_{COHSEX}$ in Eq. 4 is a self-consistent Hamiltonian, namely it depends on the solution of the time-dependent Schrödinger equation. Under the assumption of Eq. A5, it is easy to see that the COHSEX Hamiltonian under time-reversal symmetry transforms as $\hat{H}_{COHSEX}(\mathbf{r},\mathbf{r}',t) = \hat{H}^*_{COHSEX}(\mathbf{r},\mathbf{r}',-t)$. This property is consistent with the derivation of this appendix. Indeed for the COHSEX Hamiltonian Eq. A2 would become

$$-i\frac{d\phi_{v\mathbf{k}}(\mathbf{r},-t)}{dt} = \int \hat{H}_{COHSEX}(\mathbf{r},\mathbf{r}',-t)\phi_{v\mathbf{k}}(\mathbf{r},-t)d\mathbf{r}' = \int \hat{H}^*_{COHSEX}(\mathbf{r},\mathbf{r}',t)\phi_{v\mathbf{k}}(\mathbf{r},-t)d\mathbf{r}' \tag{A7}$$

and Eq. A3 remains unchanged, when a complex conjugate operation is applied. Since $\phi_{v\mathbf{k}}(\mathbf{r},t) = \phi^\circ_{v\mathbf{k}}(\mathbf{r}) + \phi'_{v\mathbf{k}}(\mathbf{r},t)$ the properties in Eqs. A5-A6 are still valid for perturbed orbitals, namely $\phi'_{v-\mathbf{k}}(\mathbf{r},t) = \phi'^*_{v\mathbf{k}}(\mathbf{r},-t)$ and $\phi'_{v-\mathbf{k}}(\mathbf{r},\omega) = \phi'^*_{v\mathbf{k}}(\mathbf{r},\omega)$. For this reason, assuming the time-reversal symmetry in the external time-dependent potential, the perturbed density matrix in Eq. 12 can be considered as real. Furthermore, since for every perturbed orbital at $\mathbf{k}$ we can obtain the corresponding $-\mathbf{k}$ by a simple complex conjugate operation, the total cost of the calculation is significantly decreased (except of the Γ point and the k-points at the boundaries).

* Electronic mail: drocca@ucdavis.edu

[1] G. Onida, L. Reining, and A. Rubio, Rev. Mod. Phys. **74**, 601 (2002).
[2] See, e.g. D. P. Hagberg, J.-H. Yum, H. Lee, F. De Angelis, T. Marinado, K. M. Karlsson, R. Humphry-Baker, L. Sun, A. Hagfeldt, M. Grätzel, and M. K. Nazeeruddin, J. Am. Chem. Soc. **130**, 6259 (2008).
[3] B. M. Kayes, M. A. Filler, M. C. Putnam, M. D. Kelzenberg, N. S. Lewis, and H. A. Atwater, Applied Physics Letters **91**, 103110 (2007).
[4] E. C. Garnett and P. Yang, J. Am. Chem. Soc. **130**, 9224 (2008).
[5] E. Runge and E. K. U. Gross, Phys. Rev. Lett. **52**, 997 (1984).
[6] S. Albrecht, L. Reining, R. Del Sole, and G. Onida, Phys. Rev. Lett. **80**, 4510 (1998).
[7] M. Rohlfing and S. G. Louie, Phys. Rev. B **62**, 4927 (2000).
[8] L. X. Benedict, E. L. Shirley, and R. B. Bohn, Phys. Rev. B **57**, R9385 (1998).
[9] D. Rocca, D. Lu, and G. Galli, J. Chem. Phys. **133**, 164109 (2010).
[10] B. Walker, A. M. Saitta, R. Gebauer, and S. Baroni, Phys. Rev. Lett. **96**, 113001 (2006).
[11] D. Rocca, R. Gebauer, Y. Saad, and S. Baroni, J. Chem. Phys. **128**, 154105 (2008).
[12] H. F. Wilson, F. Gygi, and G. Galli, Phys. Rev. B **78**, 113303 (2008).
[13] H. F. Wilson, D. Lu, F. Gygi, and G. Galli, Phys. Rev. B **78**, 113303 (2009).
[14] S. Baroni, S. de Gironcoli, A. Dal Corso, and P. Giannozzi, Rev. Mod. Phys. **73**, 515 (2001).
[15] D. Rocca, Z. Bai, R.-C. Li, and G. Galli, J. Chem. Phys. (in press) (2012).
[16] L. Hedin, Phys. Rev. **139**, A796 (1965).
[17] O. B. Malcıoğlu, R. Gebauer, D. Rocca, and S. Baroni, Comput. Phys. Commun. **182**, 1744 (2011).
[18] F. Gygi and A. Baldereschi, Phys. Rev. B **34**, 4405 (1986).
[19] H.-V. Nguyen and S. de Gironcoli, Phys. Rev. B **79**, 205114 (2009).
[20] G. Strinati, Phys. Rev. B **29**, 5718 (1984).
[21] M. S. Hybertsen and S. G. Louie, Phys. Rev. Lett. **55**, 1418 (1985).
[22] M. S. Hybertsen and S. G. Louie, Phys. Rev. B **34**, 5390 (1986).
[23] W. Kang and M. S. Hybertsen, Phys. Rev. B **82**, 195108 (2010).
[24] R. Car, E. Tosatti, S. Baroni, and S. Leelaprute, Phys. Rev. B **24**, 985 (1981).
[25] F. Bassani and G. Pastori Parravicini, *Electronic States and Optical Transitions in Solids* (Pergamon, Oxford, 1975).
[26] P. Giannozzi, S. Baroni, N. Bonini, M. Calandra, R. Car, C. Cavazzoni, D. Ceresoli, G. L. Chiarotti, M. Cococcioni, I. Dabo, et al., J. Phys.: Condens. Mat. **21**, 5502 (2009).
[27] J. P. Perdew and A. Zunger, Phys. Rev. B **23**, 5048 (1981).
[28] The Quantum Espresso pseudopotential library is available online at the URL `http://www.quantum-espresso.org/pseudo.php`. In this work the pseudopotential file `Si.pz-vbc.UPF` was used for silicon and `C.pz-vbc.UPF` for carbon.
[29] A. Dal Corso, S. Baroni, and R. Resta, Phys. Rev. B **49**, 5323 (1994).
[30] R. R. L. Zucca and Y. R. Shen, Phys. Rev. B **1**, 2668 (1970).
[31] S. Baroni and R. Resta, Phys. Rev. B **33**, 7017 (1986).
[32] H. J. Monkhorst and J. D. Pack, Phys. Rev. B **13**, 5188 (1976).
[33] A. Dal Corso, in *Quantum-Mechanical Ab-initio Calculation of the Properties of Crystalline Materials*, edited by C. Pisani (Springer Verlag, Berlin, 1996), p. 77.
[34] M. Grüning, A. Marini, and X. Gonze, Nano lett. **9**, 2820 (2009).
[35] V. Olevano and L. Reining, Phys. Rev. Lett. **86**, 5962 (2001).
[36] P. Lautenschlager, M. Garriga, L. Vina, and M. Cardona, Phys. Rev. B **36**, 4821 (1987).
[37] A. Marini, C. Hogan, M. Grüning, and D. Varsano, Comput. Phys. Commun. **180**, 1392 (2009).
[38] S. Albrecht, L. Reining, G. Onida, V. Olevano, and R. Del Sole, Phys. Rev. Lett. **83**, 3971 (1999).
[39] P. H. Hahn, K. Seino, W. G. Schmidt, J. Furthmüller, and F. Bechstedt, Physica Status Solidi B Basic Research **242**, 2720 (2005).
[40] K. H. Hellwege and O. Madelung, eds., *Numerical Data and Functional Relationships in Science and Technology*, vol. 17a and 22a of Landolt-Börnstein, New Series, Group III (Springer Verlag, Berlin, 1982).
[41] R. A. Roberts and W. C. Walker, Phys. Rev. **161**, 730 (1967).
[42] H. R. Phillip and E. A. Taft, Phys. Rev. **136**, A1445 (1964).
[43] S. Botti, F. Sottile, N. Vast, V. Olevano, L. Reining, H.-C. Weissker, A. Rubio, G. Onida, R. Del Sole, and R. W. Godby, Phys. Rev. B **69**, 155112 (2004).
[44] S. Logothetidis and J. Petalas, Journal of Applied Physics **80**, 1768 (1996).
[45] M. Rohlfing and J. Pollmann, Phys. Rev. B **63**, 125201 (2001).